Effect of Various Periodic Surface Concepts for Numerical Investigation of Flow Field Through Variable Area LP Turbine Nozzle

Hardikkumar Bhavsar and Chetankumar Mistry

Abstract The gas turbine engine performance can be improved in off-design condition by using variable area nozzle turbine (VANT) concept as mass flow rate varies in off-design conditions. In order to analyze the flow field through VANT, second-stage LPT nozzle geometry was selected from EEE proposed by Pratt and Whitney, and its endwalls were modified. In the present study, meshing of the nozzle domain was done in ICEM CFD® due to the limitation of TurboGrid® which is discussed. For the numerical analysis, two-passage and one-passage fluid models were analyzed. It was found from two-passage analysis that due to the 3D geometry of the vane at LE, incidence effect was not properly captured. Hence, flow physics is not identical in two passages. Further, one-passage numerical analysis with and without varying the periodic surfaces at −5°, 0°, and + 5° vane setting angle is performed. The results were analyzed in terms of static pressure field in the part clearances and total pressure loss coefficient. It is found that mass flow averaged total pressure loss coefficient changes within 3% range with change of different periodic surface concepts.

Nomenclature

C_{ax}	Axial chord
C_{pt}	Total pressure loss coefficient $= \frac{\overline{p_{0,\mathrm{in}}} - p_0}{\overline{p_{0,\mathrm{in}}} - \overline{p_{\mathrm{in}}}}$
C_{ps}	Static pressure coefficient $= \frac{p - \overline{p_{\mathrm{in}}}}{\overline{p_{0,\mathrm{in}}} - \overline{p_{\mathrm{in}}}}$
p	Static pressure
$\overline{p_{in}}$	Mass flow averaged inlet static pressure
p_0	Total pressure
$\overline{p_{0,in}}$	Mass flow averaged inlet total pressure
EEE	Energy-efficient engine
LE	Leading edge

H. Bhavsar (✉) · C. Mistry
Department of Aerospace Engineering, Indian Institute of Technology, Kharagpur, West Bengal, India
e-mail: csmistry@aero.iitkgp.ac.in

© The Author(s), under exclusive license to Springer Nature Singapore Pte Ltd. 2023

G. Sivaramakrishna et al. (eds.), *Proceedings of the National Aerospace Propulsion Conference*, Lecture Notes in Mechanical Engineering,
https://doi.org/10.1007/978-981-19-2378-4_8

LPT	Low-pressure turbine
LV	Leakage vortex
PS	Pressure surface
PSHSV	Pressure side horseshoe vortex
PV	Passage vortex
SS	Suction surface
SSHSV	Suction side horseshoe vortex
TE	Trailing edge
VANT	Variable area nozzle turbine

1 Introduction

The gas turbine engine is composed of several components. The performance of these components is dependent on the 3D, complex flow passing through their passage. In order to improve the performance of the components, flow physics of each components needs to be understood. This can be done by performing measurement of several parameters on the actual engine components. However, this task is very difficult as well as expensive. Also, in order to develop testing facility, it is a prior requirement to decide which parameters are required to measure and at which location. This can be understood by performing detail computational study on the selected component.

It is known that gas turbine engines are being used in several applications. Also, demand of shaft/thrust power of the gas turbine engine changes with time and operating conditions. Hence, for a quite vast period of life, engine needs to perform in the off-design condition where its mass flow requirement changes. This affects the performance of the engine. In order to operate engine near its design conditions, component flow area is required to change with change in mass flow rate. Variable area nozzle turbine (VANT) concept actively controls the performance of the gas turbine engine with change in power demand suggested by Roy-Aikins [1]. Karstensen and Wiggins [2] described the successful use of variable power turbine nozzle in various applications. Moffit et al. [3] investigated the VANT concept in single-stage turbine by varying the stator area from 70 to 130%. They found that turbine efficiency reduces at a given pressure ratio as vane setting angle was changed from design angle. Razinsky and Kuziak [4] used variable nozzle power turbine concept in GT 225 for various operating point including braking position. They observed improvement in specific fuel consumption at part-load condition as turbine inlet temperature can be kept higher. However, for mechanical movement of the vanes, part clearances are required to be accommodated near hub as well as tip endwalls and vane ends. These part clearances near both ends are responsible for occurrence of leakage flow due to the pressure gradient from PS to SS of the vane. Further, part of the leakage flow passing near the vane end surfaces has rotationality, which forms the leakage vortex within the nozzle passage. This leakage vortex mixes with the primary flow and passage vortex and increases the losses at the exit of the

nozzle. Razinsky and Kuziak [4] also observed increase in the efficiency of 0.7–4.0% when they sealed the vane ends.

Various researchers have performed study to analyze the leakage flow through turbine tip clearances. They have also concluded that 30% losses in the turbine passage are due to tip leakage flow. Hence, several studies have also been performed to mitigate or minimize the tip leakage flow by various methods. However, prior to apply some technique to inhibit the leakage flow, leakage flow field needs to be analyzed. For the VANT concept, as part clearances are required near hub and tip of the vane, leakage flow field needs to be analyzed at both the locations. Hence, present study aims to numerically investigate the leakage flow field near hub as well as tip clearance for the VANT concept. In the present study, second-stage 3D vane of the LPT from EEE proposed by Prat and Whitney was selected. Details of which are given by Leach et al. [5]. The details about turbine stage and cascade are shown in Table 1. The effect of free stream turbulence and incidence angle on the selected original geometry was performed and reported by Bhavsar and Mistry [6]. Further, for the VANT, vane pivot is present in the either part clearances which also influences the flow within the part clearances. The modification of the hub and casing endwalls for VANT concept was done and reported by Bhavsar and Mistry [7]. In the ANSYS TurboGrid®, it was not possible to define the vane with the pivot in either clearances for the domain discretization to numerically solve the flow field. Hence, fluid flow domain needs to be defined with periodic surfaces in the ICEM CFD® consisting of one or two passages. So far, various CFD studies for linear as well as annular cascade are reported, which mainly focus on the effect of change of incidence angles. In this study, as the vane is turned for the VANT concept, effect of periodic surface needs to be analyzed. Tallman and Lakshminarayana [8] used two passages for their numerical investigation on linear cascade using numerical method given by Basson and Lakshminarayana [9]. They defined one full blade, the periodic surface adjacent to PS of the central blade was formed as SS, and the periodic surface adjacent to SS of the central blade was formed as PS up to tip clearance region. In the tip clearance region, they define the periodic surface as mean camber line on both sides of the main blade.

Hence, in the present study, fluid domain with two passages (case—a) and one passage (cases b and c) was selected for the numerical analysis. Further, in case—b, periodic surfaces of fluid domain were kept constant as vane settling angle was

Table 1 Cascade and turbine parameters

	Hub	Quarter hub	Mean	Quarter tip	Tip
Inlet metal angle	32.7°	37.2°	41.7°	47.7°	52.2°
Exit metal angle	27.7°	21.5°	21°	20.5°	19.8°
Axial chord	4.907 cm				
Aspect ratio	2.65				
Flow coefficient	0.76				
Mean reaction	0.45				

changed. The case—b was not able to accommodate the variation of vane setting angle beyond ± 7°. Whereas in case—c, periodic surfaces were also varied with vane setting angle, and hence, it enables to investigate variation in vane setting angle beyond ± 7°.

2 Numerical Setup

This section discusses the construction of fluid flow model for three cases. It is followed by multiblock domain discretization in ICEM CFD® and is discussed with their limitations. The boundary conditions are discussed at the end of this section.

2.1 Fluid Flow Model

The fluid flow model with two passages is shown in Fig. 1a and denoted as case—a throughout the text. In this model, one 3D vane was placed and adjacent vanes were modeled as SS and PS at an angular pitch distance away from central vane. Hence, this model was able to capture the effect of vane turning for wide range of different setting angles. However, the fluid model of case—a has certain limitations in terms of domain discretization and effect of incidence angle as 3D vane in the annular passage was being analyzed here. This is discussed in the subsequent sections. The fluid model with one passage was analyzed having periodic surfaces at half angular pitch distance from the vane with two different cases, i.e., b and c.

In the case—b, the periodic surface was constructed using mean camber line and was kept for design vane setting angle as shown in Fig. 1b. Hence, this methodology imposes limit to perform numerical analysis on the vane setting angle beyond ± 7°. Further, in the case—c, periodic surface was constructed from mean camber line, and it was also changed with vane setting angle as shown in Fig. 1c.

2.2 Domain Discretization

In the present study, as mentioned earlier, part clearance flow field through VANT is numerically analyzed. Also, for VANT, pivot is an essential part which influences the part clearance flow field. Hence, multiblock domain discretization was done in the ICEM CFD®. H-type topology was used within the passage, and *O*-type topology was used near LE, TE, and around the pivot. From the grid sensitivity test performed in the previous study, a total of 40 elements were selected to be kept in the part clearance for all the cases. However, based on the change of geometry, minor re-distribution of the grid elements was done in various directions in each case. Overall comparison of number of elements is given in below Table 2. It is observed that case—a with

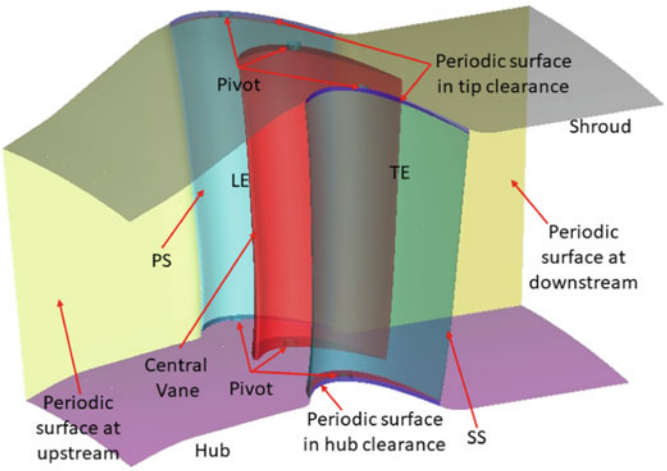

(a) For two passages (case – a)

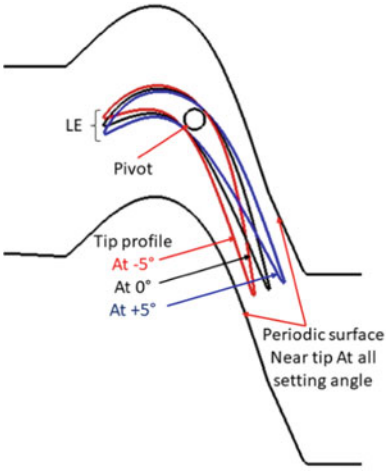

(b) For single passage (case – b)

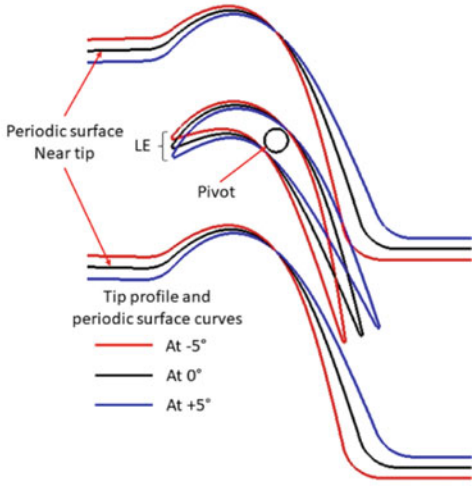

(c) For single passage (case – c)

Fig. 1 Fluid domain definition for various cases

Table 2 Overall element count

	Case—a	Case—b	Case—c
Elements (millions)	6.88	3.2	4.3

two passages required 60% more elements than case—c. Hence, it demands more computational power and/or time. The discrepancy in the number of elements from case—b to case—c was due to the increase of spanwise number of grid elements. However, it is required to be noted that in the part clearances, all cases have same

number of elements. Further, limitation to analyze wide VANT setting angle range was limited as discussed in the previous sub-section for case—b.

2.3 Boundary Condition

The steady-state RANS equations were solved in commercially available software ANSYS CFX®. For the turbulence closure, two-equation shear stress transport (SST) model was selected. The experimental investigations are planned at IIT Kharagpur using sector annular cascade tunnel based on the present numerical study. Hence, boundary conditions were selected based on the real experimental condition. The inlet velocity of 50 m/s was given with the flow component based on the vane metal angle. The outlet static pressure was given as the atmospheric pressure, i.e., 101,325 Pa. All the walls, i.e., hub and casing endwall, vane surface, and pivot surfaces were given as adiabatic no-slip condition. The periodic surfaces were given as rotational periodic. Further, the RMS convergence criteria were kept as 10^{-6}, and pressure ratio across the passage was also monitored.

3 Results and Discussion

In this section, numerical results are analyzed for the various cases initially. The limitation of case—a to not properly capture the incidence effect in different passage is discussed first. The results of case—b are thoroughly discussed by Bhavsar and Mistry [7]. However, as mentioned earlier, using case—b analysis of $\pm$ 10° setting angle change was not able to perform. Hence, detailed flow field for $-10°$ to $+$ 10° setting angle change is discussed using geometry made by case—c.

3.1 Case—a

The flow field through two-passage case for design setting angle is shown in Fig. 2a and b using total pressure loss coefficient, C_{pt} near casing, and hub endwall, respectively. The C_{pt} contour at 0, 50, and 100% C_{ax} location from LE of the vane is shown. In Fig. 2a, total pressure loss due to the formation of the horseshoe vortex is observed near the casing endwall. However, it can be observed that the formation of the horseshoe vortex in both the passages is not identical.

This is denoted by $A1$ and $A2$ in the streamwise plane of Fig. 2a at LE of the vane. Further, the formation of the leakage vortex is also differed in streamwise plane shown at 50% C_{ax} distance downstream of the LE. It is observed that the leakage vortex in the region denoted by $B1$ is extended tangentially away from the suction side compared to leakage vortex denoted by $B2$. However, core of the leakage vortex

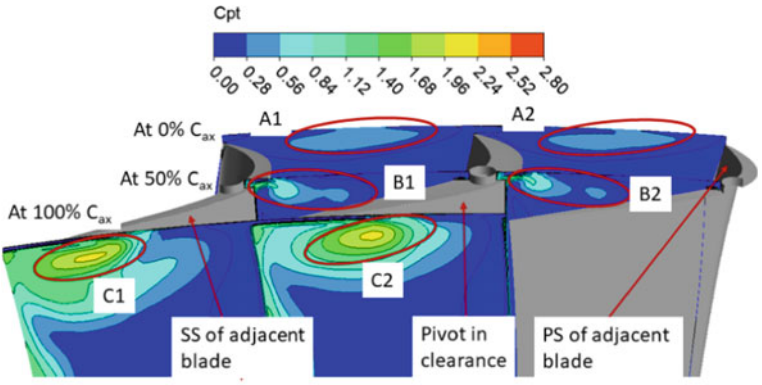

(a) near casing endwall

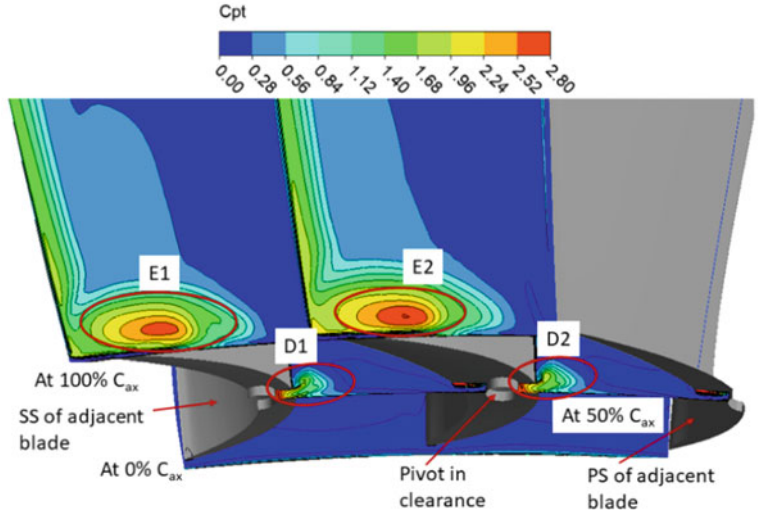

(b) near hub endwall

Fig. 2 Streamwise C_{pt} contour

remains near the SS as shown by $B1$. The significant effect of this can be observed in the plane located at TE of the vane. It is observed that the core of the total pressure loss region is elongated in the tangential direction as shown by $C1$. However, as leakage vortex (dented by $B2$) was away from the SS at 50% C_{ax} location, total pressure loss region in the plane at TE is shifted away from the SS (denoted by $C2$).

Figure 2b shows the C_{pt} contour at similarly located plane near hub endwall. The plane located at LE of the vane does not show much discrepancy. The formation of leakage vortex differs minutely from each other at 50% C_{ax} location downstream of vane LE. The plane located at TE of the vane shows higher total pressure loss in the core shown by $E2$ compared to $E1$.

As the two passages are numerically analyzed, ideally contours should be identical in both the passages. However, the present numerical analysis is not able to capture ideal behavior. This can better be illustrated by observing the velocity distribution at different spanwise locations. It gives the effect of differences in flow incidence at the LE of central vane and partially modeled adjacent vanes. The Mach number contours at 25, 50, and 75% spanwise locations are shown in Fig. 3a–c, respectively.

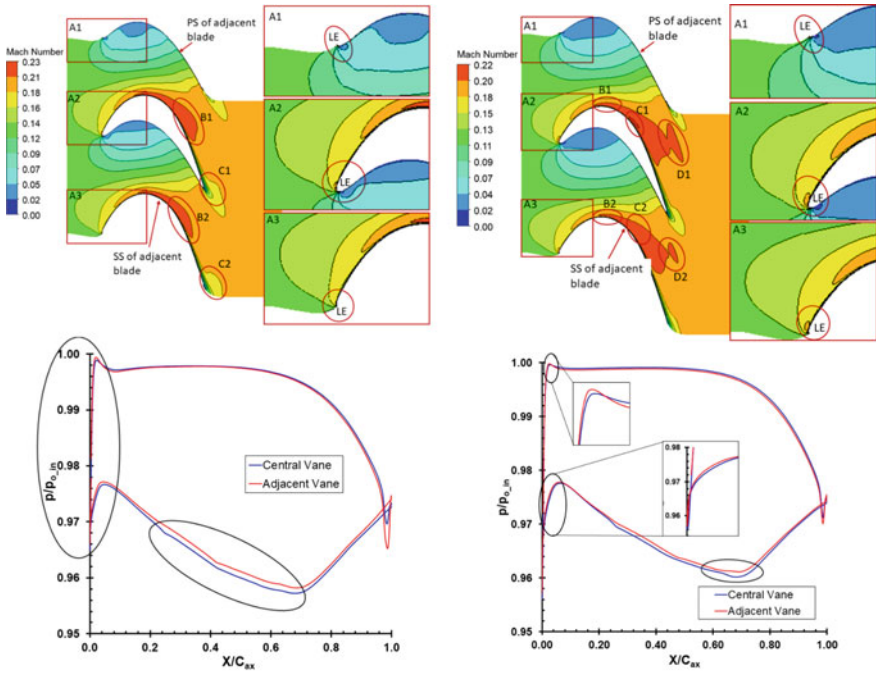

(a) at 25% span

(b) at 50% span

(c) at 75% span

Fig. 3 Mach number contour at different spanwise locations

The enlarged view of LE of adjacent vane PS is denoted by $A1$, LE of central vane is denoted by $A2$, and LE of adjacent vane SS is denoted by $A3$ in all the figures.

Figure 3a shows the Mach number contour (upper part) and loading distribution (below part) at 25% span location. The discrepancy in the Mach number distribution at LE of central vane and adjacent vanes is clearly visible. From region denoted by $A1$, it is observed that on the PS of adjacent vane, flow accelerates just downstream of the LE and it again decelerates around 15% C_{ax} location from LE. However, $A2$ region shows that flow gradually accelerates downstream of LE on the PS of the central vane. Further, on the SS of central vane (region denoted by $A2$), minute region of acceleration is observed which is followed by deceleration, and around 15% C_{ax} location downstream of LE acceleration on the SS is observed. However, this kind of behavior is not observed on the SS of adjacent vane shown by region $A3$. Also, acceleration of the flow on the SS of central vane is observed earlier than on the SS of the adjacent vane. This change of flow incidence at the LE of central and adjacent vane affects the flow physics within the passage. However, these effects are clearly observed on the SS of the vane which are denoted by $B1$ and $B2$ near the throat and $C1$ and $C2$ near TE of the vane. This can also be seen from the pressure distribution shown in the below part of Fig. 3a.

Figure 3b shows the Mach number distribution at 50% span location. From $A1$ and $A2$ regions, it can be observed that on the PS, downstream of the LE, slightly larger extent of flow deceleration region is observed on the central vane compared to adjacent vane. This can also be seen in loading distribution shown in below part of the figure. This is seen by reduction of pressure value in the loading distribution. Further, on SS, downstream of the LE, larger extent of flow acceleration region is observed on the central vane compared to adjacent vane shown in $A3$. Due to this minor discrepancy in the incidence angle on the central and adjacent vanes, early acceleration at $B1$ is observed compared to $B2$. Similarly, higher Mach number in $C1$ region is seen compared to $C2$. Also, near TE, acceleration of larger portion of flow in the tangential direction is observed, which is denoted by $D1$ compared to $D2$.

Figure 3c shows the Mach number distribution at 75% span location. Here, discrepancies observed are: near LE, on PS of adjacent blade and central blade; early acceleration in $B2$ region compared to $B1$ region; and larger extent of acceleration in $C2$ region compared to $C1$ region.

Hence, from the above observed phenomenon, it can be concluded that numerical analysis of required vane turning angle for the VANT concept can be accommodated. Further, simulation of two passages requires 60% more grid elements compared to single passage as mentioned earlier. The increase in the number of grid elements increases the computational cost. However, the numerical results show that the flow field in both the passages is not identical. Hence, in the present study, further investigations of flow field are done using one-passage method.

3.2 Comparison of Case—B and Case—C

The comparison of numerical results obtained for case—b and case—c is discussed using Mach number contours. Due to the geometrical constraint of case—b, the comparison for −5°, 0°, and + 5° vane turning angle is shown by Mach number contour at 50% span location in Fig. 4.

It should be noted that actual domain was made for one passage only. However, for better visualization, two passages are shown using instant transform tool of ANSYS CFD Post®. For all vane turning angles, it can be observed that most of the flow features are captured quite similar in both the cases. However, minor discrepancy is observed between cases b and c near LE and in the wake region for −5° vane

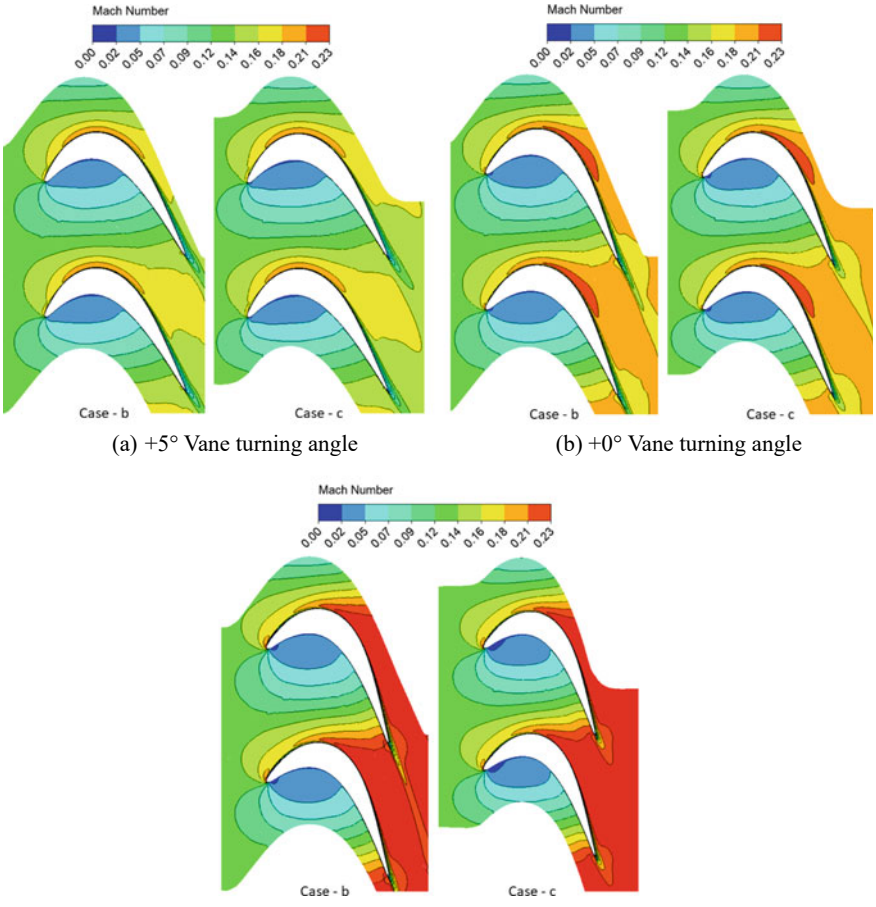

(a) +5° Vane turning angle

(b) +0° Vane turning angle

(c) -5°Vane turning angle

Fig. 4 Comparison of Mach number contour at 50% span for case—b and case—c

turning angle. It should be noted that both the cases were discretized and simulated individually. Hence, computational error of the numerical solution might lead to such small discrepancies in the Mach number contours. Further, it is seen that as the vane setting angle is changed from + 5° to −5°, the throat area reduces and Mach number increases.

The static pressure coefficient—C_{ps} comparison between case—b and case—c in the hub as well as tip side part clearances are shown with velocity vectors in Figs. 5 and 6, respectively. Figure 5a–c shows the C_{ps} contour for + 5°, 0°, and − 5° setting angles. As the vane setting angle is changed from + 5° to −5°, the throat area reduces. Hence, flow velocity increases within the passage and static pressure reduces. Also, the throat area shifts from 73% C_{ax} to 84% C_{ax} location downstream of the LE as vane setting angle changed from + 5° to −5°. The leakage flow through the hub side part clearance occurs due to the presence of pressure gradient from PS to SS. The maximum pressure gradient for the leakage flow to be occurred is observed near PS of the vane in both hub as well as tip side part clearances. The flow gets deflected due to the presence of the circular pivot in the part clearance. Hence, flow recirculation region is observed toward the SS from the pivot. This region is denoted by the 'RC' in all the figures. The recirculation region reduces in extent as vane setting angle is changed from + 5° to −5°. Further, the presence of pivot puts discontinuity in the favorable pressure gradient near PS. The favorable pressure gradient region in the upstream of the pivot is denoted by $A1$ and in the downstream of the pivot is denoted by $A2$. There is a greater effect of vane turning angle observed on the region $A2$ compared to $A1$. As the vane turning angle is changed from + 5° to −5°, the magnitude and extent of favorable pressure gradient increase significantly in the downstream direction of the pivot location, i.e., region $A2$.

The C_{ps} distribution for the case—b and case—c is compared in Fig. 5a for + 5° vane turning angle. The discrepancy in the value of C_{ps} is observed mainly from the RC region to the throat region. This discrepancy reduces for the 0° vane setting angle case shown in Fig. 5b and vanishes for the −5° vane setting angle case which is shown in Fig. 5c. The difference of C_{ps} distribution in the tip side part clearances is observed between case—b and case—c for all the vane turning angles as shown in Fig. 6. This difference is clearly seen in the favorable pressure gradient region upstream of the pivot denoted by region $A1$ as well as between the RC and throat location. The difference of C_{ps} distribution near throat region reduces as vane turning angle is changed toward −5°. Further, very minor difference in the region $A2$ is observed for all the cases.

3.3 Exit Flow Field Comparison

The total pressure loss coefficient, i.e., C_{pt}, at the exit of the cascade is shown for cases—a, b, and c at + 5° vane turning angle using contour plot in Fig. 7a–c, respectively. Due to the provision of part clearances near hub and casing endwalls, leakage flow occurs and part of it forms the leakage vortex. This leakage vortex

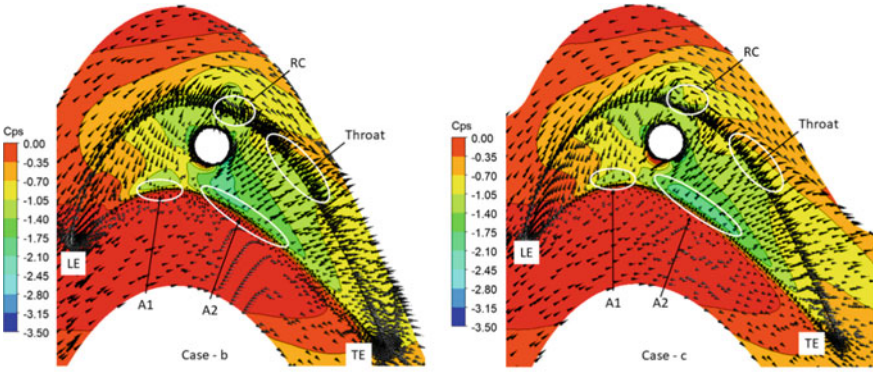

(a) +5° vane turning angle

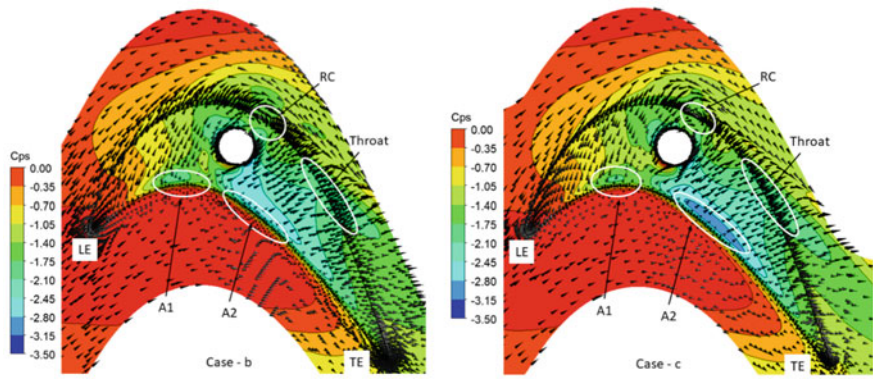

(b) 0° vane turning angle

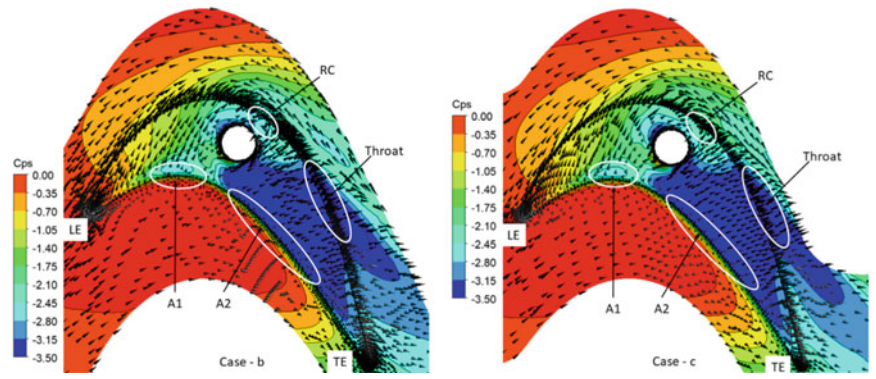

(c) -5° vane turning angle

Fig. 5 Static pressure coefficient and velocity vector in hub side part clearance

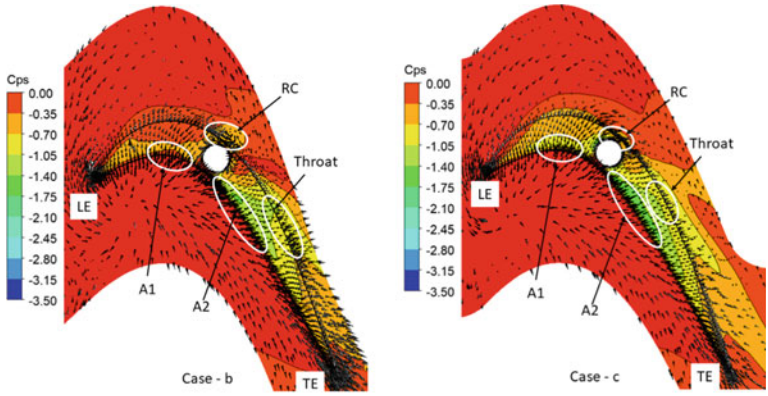

(a) +5° vane turning angle

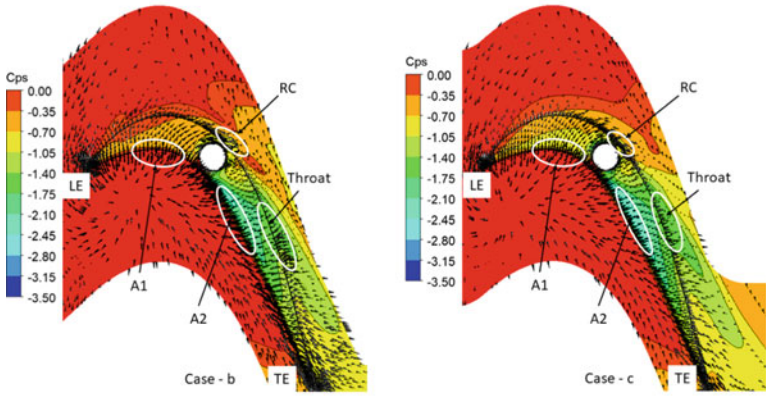

(b) 0° vane turning angle

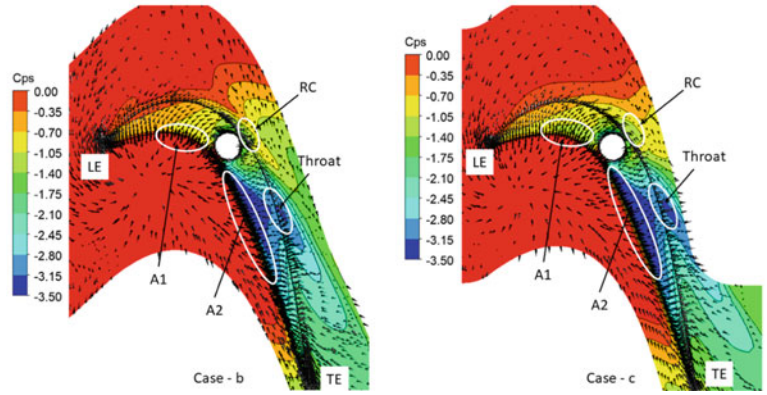

(c) -5° vane turning angle

Fig. 6 Static pressure coefficient and velocity vector in tip side part clearance

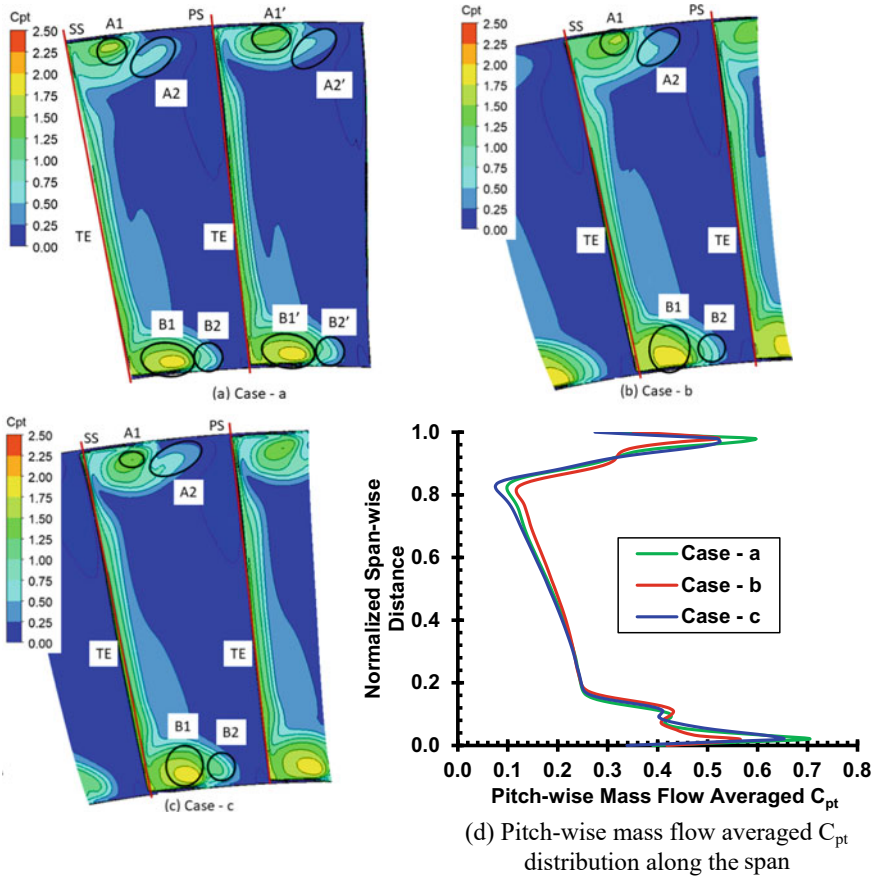

(d) Pitch-wise mass flow averaged C_{pt} distribution along the span

Fig. 7 C_{pt} comparison at the exit of the cascade for + 5° vane turning angle

merges with the passage vortex, and hence, two loss regions are seen near each endwalls. These are denoted by *A*1 and *B*1 near casing and hub endwall, respectively. It is evident that for case—a, due to the non-identical prediction of incidence angle and flow field in two different passages, total pressure loss region associated with hub and tip leakage vortex differs in size. This is denoted by *A*1 and *A*1', *A*2 and *A*2', and *B*1 and *B*1'.

It can be observed that case—b predicts the larger extent of loss core in the region *A*1. Also, near the casing endwall, larger spanwise extent of the loss region is observed for case—b, i.e., from casing endwall to 84% of span compared to case—c, i.e., up to 86% of span. However, case—c predicts the larger extent of the loss region in the tangential direction, which is denoted by *A*2. This can be observed by higher pitch-wise mass flow averaged C_{pt} value in Fig. 7d, from 92% of span to 97% of span for case—c. Further, almost similar pitch-wise mass flow averaged C_{pt} peak value is predicted at 97 and 98% of the span for case—c and case—b, respectively,

(shown in Fig. 7d) whereas case—a predicts 13% higher peak value of C_{pt}. Similar to casing endwall region, extent of the core loss region near hub endwall denoted by $B1$ reduces for case—c. The spanwise extent of the loss region is up to 16% of span for case—b compared to 14% of span for case—c, and for case—a, it is near 12% of span. However, extended loss region in the tangential direction is seen for case—c which is denoted by $B2$. Further, peak in pitch-wise mass flow averaged C_{pt} value is observed for case—a at 2% span.

Figure 8a–c shows the C_{pt} contour for cases—a, b, and c, respectively, for 0° vane turning angle. Here also, core of the loss region is not seen as identical for case—a ($A1$ and $A1'$, $A2$ and $A2'$). Near the casing endwall, larger extent of the core loss region denoted by $A1$ is observed for case—b compared to cases—a and c. Further, the loss region from casing endwall is extended up to 82.5% of span for case—b compared to 85% of span for case—a and 86.5% of span for case—c.

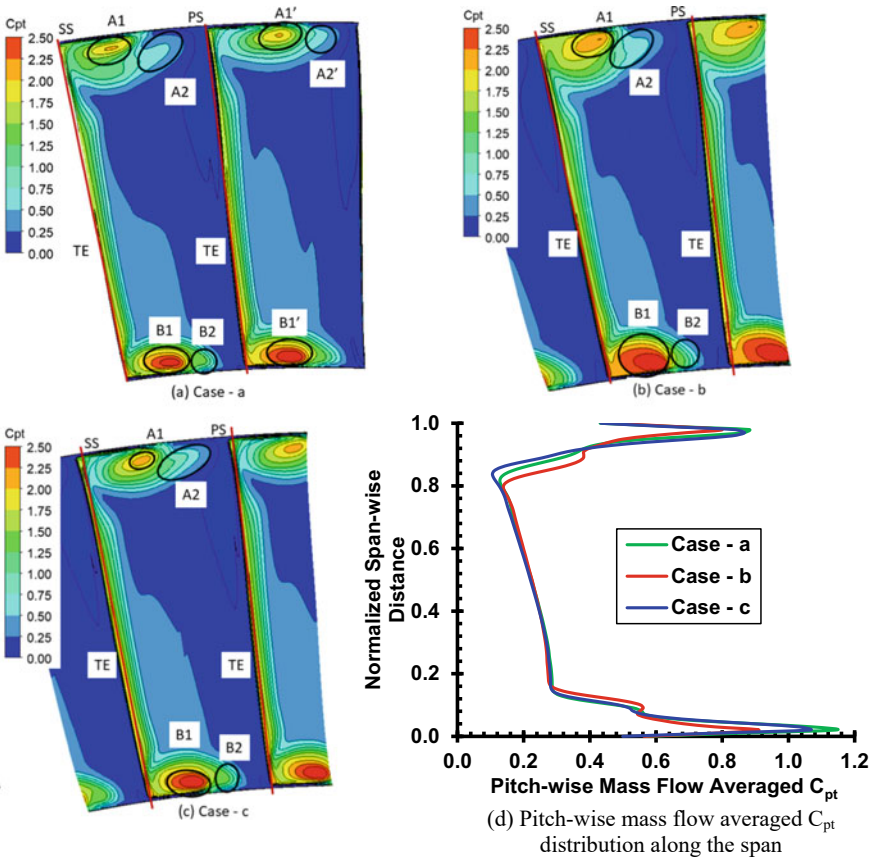

(d) Pitch-wise mass flow averaged C_{pt} distribution along the span

Fig. 8 C_{pt} comparison at the exit of the cascade for 0° vane turning angle

Also, cases—a and c predict the larger extent of loss region in the tangential direction denoted by *A*2 and *A*2' compared to case—b. Hence, higher pitch-wise mass flow averaged C_{pt} value is seen in Fig. 8d from 92% of span to peak at 97% of span for case—c and peak at 98% of span for case—b. The peak C_{pt} value increased by 8.5% near casing endwall for case—c. Further, case—a predicts even higher peak C_{pt} value by 10% at 98% span. Near the hub endwall, extent of the core loss region denoted by *B*1 reduces for case—c compared to case—b. The spanwise extent of loss region is observed up to 15% of span for case—b and 13% of span for case—c. However, for case—c, due to the larger extent of loss region denoted by *B*2 increases the pitch-wise mass flow averaged C_{pt} value from hub endwall to 7% of span. The peak C_{pt} value increases by 17% for case—c compared to case—b. Here also, case—a predicts 25% higher peak C_{pt} near hub endwall.

Figure 9a–c shows the C_{pt} contour at the exit of the cascade for cases—a, b, and c at −5° vane turning angle, respectively. Figure 9d shows the pitch-wise mass flow averaged C_{pt} distribution for both the cases along the span at the exit of the cascade.

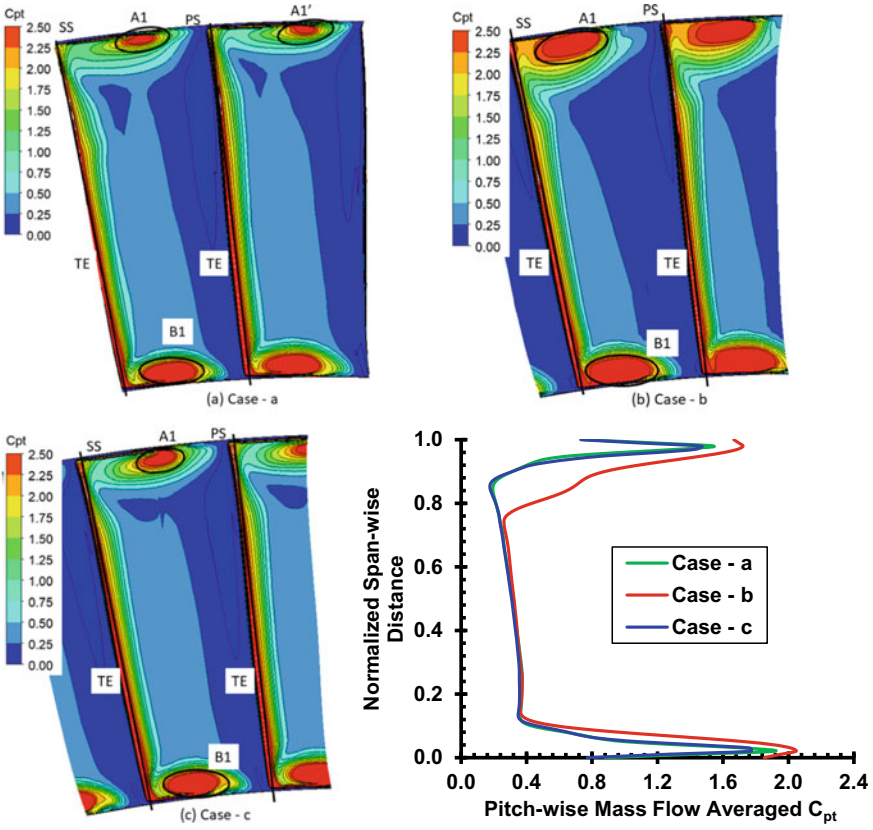

(d) Pitch-wise mass flow averaged C_{pt} distribution along the span

Fig. 9 C_{pt} comparison at the exit of the cascade for −5° vane turning angle

It is seen that core loss region near casing endwall denoted by $A1$ starts by 0.7° away from the SS for case—b compared to 1.8° away from SS for cases—a and c. Further, in the tangential direction, it occupies 2.2° for case—b compared to 1.5° and 1.4° for cases—a and c, respectively. The loss region lies from casing endwall to 84% of span for case—b compared to 88.5% of span for cases—a and c. The pitch-wise mass flow averaged C_{pt} increases from 75% span for case—b, and 17% higher peak value is predicted at 98% of span for case—b. The case—a predicts 5% higher peak C_{pt} value at 98% span. The extent of the loss region near hub is denoted by $B1$ reduces for cases—a and c insignificantly. However, peak value of mass flow averaged C_{pt} increases by 8% for case—a and by 15% for case—b compared to case—c.

The effect of change of periodic surfaces on the exit velocity flow angle is shown in Fig. 10a–c for + 5°, 0°, and −5° vane turning angle, respectively. The exit velocity flow angle changes linearly with change in vane turning angle, i.e., at + 5° vane turning angle, it is around 30°, at 0° vane turning angle, it is 25°, and at −5°, it is 20°. However, at particular vane turning angle, pitch-wise mass flow averaged exit velocity flow angle shows discrepancy from 78% span to 95%.

In order to quantify overall total pressure loss, mass flow averaged total pressure loss coefficient is obtained at the exit of the cascade for various vane turning angle in cases—a, b, and c. The obtained values are shown in Fig. 11. As already seen from the total pressure loss contour and its pitch-wise mass flow averaged distribution along the span, for −5° vane turning angle, highest total pressure loss is observed. The mass flow averaged total pressure loss reduces to minimum at + 5° vane turning angle due to reduction of mixing and viscous dissipation as kinetic energy reduces for the opening position. The case—a predicts higher losses for all vane turning angles. Also, it can be noted that the difference in the mass flow averaged C_{pt} values for various vane turning angles in cases—a, b, and c is not more than 3%. However, method used in case—c gives wide range of VANT to be analyzed with lesser number of grid points.

4 Conclusion

The present study focuses on the numerical investigation of part clearance flow field near hub as well as casing endwall for the VANT concept. In order to numerically investigate the VANT concept, three different methods were used for the modeling of periodic surface. Based on the results, certain conclusions are made which are shown below:

1. Case—a was modeled with two passages that can accommodate wide range of vane turning angle for the VANT concept. This method includes one central vane and either side adjacent vanes were partially modeled with PS/SS. As the

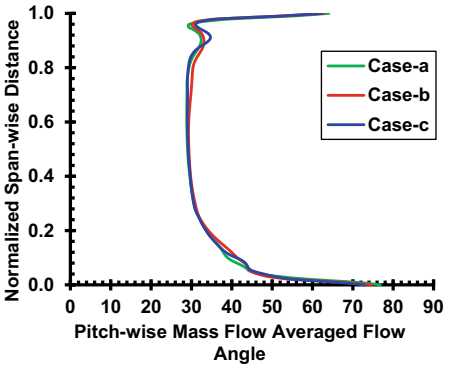

(a) +5˚ vane turning angle

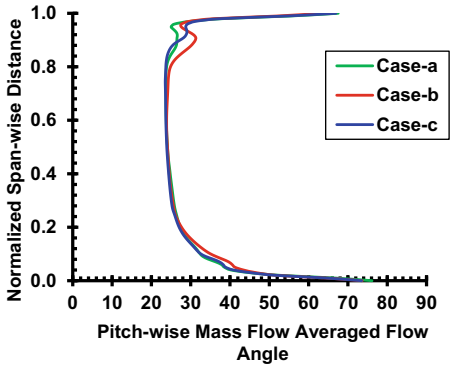

(b) 0˚ vane turning angle

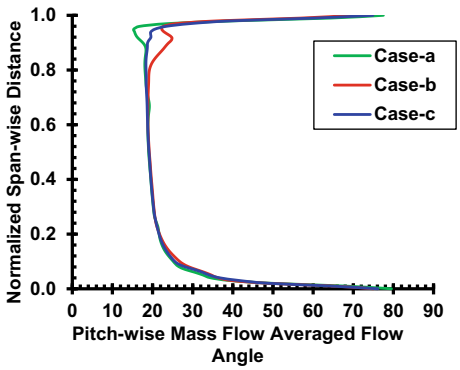

(c) -5˚ vane turning angle

Fig. 10 Exit velocity flow angle distribution

adjacent vanes were partially modeled, due to the 3D geometry of the vane, incidence angle was not captured identically in both the passages. Also, it required 60% more grid elements which increases the computation cost.

2. Case—b was modeled with one vane and constant periodic surfaces of designed setting angle at half angular pitch distance on either side of the vane. However,

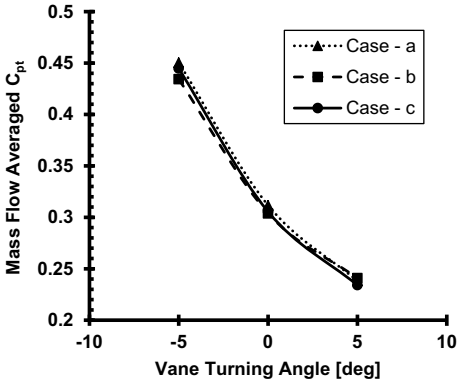

Fig. 11 Mass flow averaged C_{pt}

using this concept was not able to accommodate wide range of vane setting angle.

3. In the case—c periodic surfaces were modified as per change of vane setting angle. Hence, this method accommodates wide range of vane setting angle for the VANT concept.
4. From the comparison Mach number contour plot at 50% span location for case—b and case—c, it was observed that due to unavoidable computational errors, minor discrepancies were observed. Also, as the static pressure coefficient contours were compared in the tip side part clearance, discrepancies in the upstream part of the pivot were observed. This discrepancy reduces as the vane turning angle was changed toward $-5°$.
5. From the C_{pt} distribution at the exit of the cascade, it is seen that case—b predicts higher loss in the core of the loss region. Also, it predicts larger extent of the loss region in the spanwise direction, whereas case—c predicts larger extent in the tangential direction.
6. The difference in the overall mass flow averaged total pressure loss coefficient value at the exit of the cascade within 3% for $\pm$ 5° vane turning angles between cases—a, b, and c. This difference is 0.54% for 0° vane setting angle when periodic surfaces remain almost similar in both the cases between case—b and case—c. This difference increases between cases—a and c for 0° vane turning angle to 2%. This might be due to incorrect prediction of incidence angle in two passages and unavoidable numerical errors.

References

1. Roy-Aikins JEA (1988) A Study of variable geometry in advanced ga turbines. PhD. Thesis, Cranfield Institute of Technology
2. Karstensen KW, Wiggins JO (1989) A variable geometry power turbine for marine gas turbines. In: Gas turbine and aeroengine congress and exposition. Torronto, Ontario

3. Moffitt TP, Whitney WJ, Schum HJ (1969) Performance of a single stage turbine as affected by variable stator area. In: AIAA 5th propulsion joint specialist conference. Colorado, pp 69–525
4. Razinsky EH, Jr WRK (1977) Aerothermodynamic performance of a variable nozzle power turbine stage for an automotive gas turbine (77):587–592
5. Leach K, Thulin R, Howe D (1982) Energy efficient engine turbine intermediate case and low pressure turbine component test hardware detailed design
6. Bhavsar HM, Mistry CS (2019) Numerical study of part clearance and free stream turbulence on high end-wall LP turbine nozzle annular cascade. In: Proceeding of the ASME 2019 gas turbine India. IIT Madras
7. Bhavsar HM, Mistry CS (2020) Numerical investigations on the effect of pivot shapes in part clearance flow field of variable area LP turbine nozzle vane. In: Proceeding of the ASME 2020 turbo expo virtual conference
8. Tallman J, Lakshminarayana B (2001) Methods for desensitizing tip clearance effects in turbines. In: Proceeding of the ASME turbo expo 2001. New Orleans
9. Basson AH, Lakshminarayana B (1995) Numerical simulation of tip clearance effects in turbomachinery. ASME J Turbomach 109(4):545–549